Composites Part B 207 (2021) 108554

Contents lists available at ScienceDirect

Composites Part B

journal homepage: www.elsevier.com/locate/compositesb

Investigating the roles of fiber, resin, and stacking sequence on the low-velocity impact response of novel hybrid thermoplastic composites

M.E. Kazemi [a,b], L. Shanmugam [a], A. Dadashi [c], M. Shakouri [d], D. Lu [e], Z. Du [g], Y. Hu [g], J. Wang [g], W. Zhang [b], L. Yang [f,**], J. Yang [a,e,*]

[a] Department of Mechanical and Aerospace Engineering, The Hong Kong University of Science and Technology, Clear Water Bay, Kowloon, Hong Kong Special Administrative Region
[b] Department of Mechanical and Automation Engineering, The Chinese University of Hong Kong, Shatin, NT, Hong Kong Special Administrative Region
[c] Department of Mechanical Engineering, Semnan University, P.O. Box 35131-19111, Semnan, Iran
[d] Department of Aerospace Engineering, Semnan University, P.O. Box 35131-19111, Semnan, Iran
[e] Centre for Engineering Materials and Reliability, Guangzhou HKUST Fok Ying Tung Research Institute, Guangzhou, China
[f] College of Civil and Transportation Engineering, Shenzhen University, Shenzhen, China
[g] Guangzhou Lushan New Materials Co., Ltd., Guangzhou, China

ARTICLE INFO

Keywords:
Low-velocity impact
Hybrid composites
Thermoplastic resin
FE model
Carbon fibers
UHMWPE fibers

ABSTRACT

This study investigates the effects of fiber type, resin type, and stacking sequence on the dynamic response of fiber-reinforced polymer composite (FRPC) laminates under low-velocity impact (LVI) tests. Novel thermoplastic (TP) laminates are fabricated with a newly developed liquid methyl methacrylate thermoplastic resin, Elium® 188, at room temperature. FRPCs comprising woven ultra-high molecular weight polyethylene (UHMWPE) fabrics, woven carbon fabrics, and two different hybrid systems with alternative stacking sequences of those fibers are fabricated by the vacuum-assisted resin infusion (VARI) method. Besides, equivalent thermosetting-based (TS) composites with two epoxy systems are fabricated to compare the role of matrix type. Impact tests at different energy levels are performed on the TP and TS laminates to investigate the impact characteristics, namely contact force, deflection, energy attributes, structural integrity, and failure/damage modes. Besides, the mechanics of structure genome (MSG) and the commercial finite element code ABAQUS are used to verify the experimental results for one of the developed laminates. The results demonstrate that the hybrid system with UHMWPE fibers on the sides exhibits lower structural loss up to 47% and lower absorbed energy by 18% compared to those presented by the other type of hybrid system comprising carbon fabrics on the sides. Besides, it is found that the newly developed TP laminate underwent extended plasticity and presented a ductile behavior. The newly developed TP laminate demonstrated lower structural loss up to 200%, lower contact force by 14%, and lower absorbed energy by 48% compared to those of TS counterparts.

1. Introduction

The use of fiber-reinforced polymer composites (FRPCs) in various industries is being increased thanks to their distinct advantages, such as high specific strength and stiffness. Nonetheless, due to their brittle nature, they are prone to delamination when subjected to low-velocity impact (LVI) events, which can remarkably affect their applications [1]. LVI damage can significantly degrade the structural integrity and (residual) mechanical properties of composite structures [2]. LVI can cause various damages in FRPC laminates such as matrix cracking, debonding, delamination, and fiber breakage/failure [3]. Hence, the out-of-plane response of FRPCs should be considered when designing and fabricating such structures. Concerning the fabrication of FRPCs, various fibers/fabrics such as carbon, glass, aramid, and ultra-high molecular weight polyethylene (UHMWPE) with different resins, namely thermosetting (TS) or thermoplastic (TP) are being commonly used. Carbon fibers thanks to their tremendous in-plane mechanical properties, such as high stiffness and strength have been commonly used

* Corresponding author. Department of Mechanical and Aerospace Engineering, The Hong Kong University of Science and Technology, Clear Water Bay, Kowloon, Hong Kong Special Administrative Region.
** Corresponding author.
E-mail addresses: yanglei@szu.edu.cn (L. Yang), maeyang@ust.hk (J. Yang).

https://doi.org/10.1016/j.compositesb.2020.108554
Received 7 October 2020; Received in revised form 27 November 2020; Accepted 2 December 2020
Available online 8 December 2020

in manufacturing aerospace structures [4–6]. However, due to the low toughness of carbon fibers, they show vulnerable (brittle) behavior in LVI applications, which can remarkably reduce residual compressive properties of FRPCs and threaten the integrity of structures [7]. In order to alleviate such a problem, hybridizing with other fibers such as glass or aramid is commonly adopted, which can increase flexibility, resulting in improved impact performance [8]. Moreover, the weight and cost of structures, fabricated with a single fiber type can be reduced by hybridization [9].

However, hybridizing with glass fibers increases the weight of carbon-based FRPCs, although providing a great extent of flexibility [10]. Hence, to reduce the weight, researchers replaced glass fibers with aramid fibers [8]. To further decrease the weight and improve the low-velocity and high-velocity impact characteristics of FRPCs, UHMWPE fibers have been introduced for manufacturing composite structures [11]. UHMWPE fibers are (synthetic) thermoplastic materials, which possess ductile behavior and are excellent for impact applications. They can absorb much higher energy than that of carbon, glass, or aramid fibers. Furthermore, their density is much lower than that of those fibers [12]. However, they have low stiffness (about 5 GPa for their composite systems) when compared with high-stiffness carbon fibers (about 60 GPa for their composite systems [13]). In addition, UHMWPE fibers cannot be used at high temperatures (above 120 °C) applications, and also cannot be solely used in applications that require high stiffness. As a result, the combination of UHMWPE/carbon fibers as hybrid FRP composite systems can be formulated to provide optimum stiffness, strength, and energy absorption characteristics for miscellaneous applications.

Most of the studies in the literature are mainly based on using TS resins. Despite the fact that TS resins provide excellent in-plane mechanical properties with a medium to high curing temperature range, they show poor impact properties. As a result, TP resins are being used to manufacture FRPC structures for impact applications, which can also be recycled. TP FRPC laminates have shown improved damage tolerance and impact performance compared to those of thermosetting counterparts. However, due to the solid state of traditional TP resins (namely PEEK), vacuum-assisted resin infusion (VARI) cannot be used for fabrication, as those resins need to reach elevated temperatures to flow and cure, which is only possible by using expensive equipment and high processing temperatures. In order to tackle this issue, Arkema company has recently introduced a novel acrylic methyl methacrylate thermoplastic resin, Elium®, which is liquid at room temperature and can be used in the VARI process to increase the production rate and decrease labor and manufacturing costs [14]. To this date and to the best of the authors' knowledge, the low-velocity impact behavior of thermoplastic hybrid TP laminates fabricated at room temperature has not yet been investigated. For this, plain weave UHMWPE fabrics, carbon fabrics, and their hybrid systems with alternating layers of carbon and UHMWPE fabrics (one system with carbon fabrics on the sides and UHMWPE fabrics in the middle, and the other one with UHMWPE fabrics on the sides and carbon fabrics in the middle) are manufactured with Elium® resin to study the influence of stacking sequence on the LVI characteristics. Moreover, thermosetting (epoxy) resins (Epolam and Sikafloor®) are utilized to manufacture equivalent TS FRPC counterparts to investigate the influence of the resin type. LVI tests at different energy levels are followed to investigate and compare the impact contact force, displacement, energy attributes, structural integrity, and failure modes among the laminates. Moreover, the mechanics of structure genome (MSG) [15] and the commercial finite element code ABAQUS/Explicit are combined and applied for one of the tested laminates to validate the experimental results.

2. Experimental procedure

Plain weave ultra-high molecular weight polyethylene (UHMWPE, denoted by PEf) and carbon fabrics (denoted by Cf) are used for fabricating fiber-reinforced polymer composite (FRPC) laminates. UHMWPE QuantaFlex™ fabrics are provided by Quantumeta, and Hexforce 282 carbon fabrics are provided from Hexcel. The areal densities of the carbon and UHMWPE fabrics are 197 g/m^2 and 172 g/m^2, respectively. The thicknesses of the carbon and UHMWPE fabrics are 0.26 mm and 0.35 mm, respectively. Two thermosetting (TS) resins, including Sikafloor® and Epolam (with similar mechanical characteristics) and a thermoplastic (TP) liquid resin, Elium® 188 are chosen to fabricate the laminates. For epoxy Epolam 5015 resin, Epolam hardener 5015 with the mixing ratio by weight of (hardener to resin) 30–100 is used. For Sikafloor® 156, its hardener with the mixing ratio by weight of 33–100 is used. As Elium® 188 is a low viscosity thermoplastic reactive methyl methacrylate resin, 2% (by weight) of benzoyl peroxide powder is used as an initiator for polymerization to form the PMMA resin [13]. The FRPC laminates are fabricated by the VARI method at room temperature. In addition to monolithic composites with one single fiber type, two hybrid systems with alternating layers of carbon and UHMWPE fabrics (one system with carbon fabrics on the sides and UHMWPE fabrics in the middle, and the other one with UHMWPE fabrics on the sides and carbon fabrics in the middle) are fabricated (refer to group laminates 2 and 3 in Table 1). The laminates' name, stacking sequence, thickness, density, and fiber volume fraction are provided in Table 1. To perform the low-velocity impact (LVI) test, ASTM D7136 is conducted. As in this study multiple laminates with different fiber types, stacking sequence, resins and thicknesses are fabricated, based on preliminary experiments, different LVI tests at energy levels of 10 J, 15 J, 20 J, 33 J, and 40 J are selected to see different failure modes namely rebounding (with/out delamination), penetration, and perforation, which will be

Table 1
Laminates code, stacking sequence, thickness, density, and fiber volume fraction.

Laminate name	Stacking sequence[a]	Resin type	Laminate thickness (mm)	Laminate Density (gr/cm^3)	Laminate FVF[b]
1E	$(Cf)_8$	Elium® 188	1.57 ± 0.02	1.43 ± 0.03	0.58 ± 0.02
2E	$(Cf/PEf)_{2S}$	Elium® 188	2.23 ± 0.02	1.20 ± 0.02	0.50 ± 0.01
3E	$(PEf/Cf)_{2S}$	Elium® 188	2.27 ± 0.03	1.20 ± 0.02	0.50 ± 0.01
4E	$(PEf)_8$	Elium® 188	2.88 ± 0.05	1.00 ± 0.02	0.47 ± 0.01
1P	$(Cf)_8$	Epolam 5015	1.58 ± 0.03	1.45 ± 0.05	0.59 ± 0.03
2P	$(Cf/PEf)_{2S}$	Epolam 5015	2.20 ± 0.04	1.22 ± 0.04	0.52 ± 0.02
3P	$(PEf/Cf)_{2S}$	Epolam 5015	2.25 ± 0.04	1.22 ± 0.04	0.51 ± 0.02
4P	$(PEf)_8$	Epolam 5015	2.90 ± 0.05	1.01 ± 0.03	0.48 ± 0.02
1S	$(Cf)_8$	Sikafloor® 156	1.60 ± 0.02	1.46 ± 0.04	0.58 ± 0.03
2S	$(Cf/PEf)_{2S}$	Sikafloor® 156	2.26 ± 0.02	1.23 ± 0.03	0.51 ± 0.01
3S	$(PEf/Cf)_{2S}$	Sikafloor® 156	2.29 ± 0.03	1.23 ± 0.03	0.51 ± 0.01
4S	$(PEf)_8$	Sikafloor® 156	2.89 ± 0.03	1.03 ± 0.03	0.49 ± 0.01
5E	$(Cf)_{14}$	Elium® 188	2.84 ± 0.03	1.43 ± 0.03	0.63 ± 0.03

Example: $(Cf/PEf)_{2S}$: (Cf/PEf/Cf/PEf/PEf/Cf/PEf/Cf)

[a] Cf: Carbon fabric, PEf: UHMWPE fabric, $()_N$: N number of layers, $()_S$: Symmetry.

[b] FVF: Fiber volume fraction.

discussed in the results and discussion section. LVI characteristics, namely contact force, displacement, energy attributes, structural integrity, and failure modes are investigated and compared among different laminates. For each impact energy level and laminate code, three specimens with lengths of 100 mm × 100 mm are cut via an abrasive waterjet cutting machine. Then the specimens are mounted in the drop weight tower machine. For conducting the tests, each specimen is inserted in rubber-tipped clamps, providing a circular impacting area with a diameter of 76 mm.

The shape of the impactor is hemispherical with a diameter of 12.7 mm and a total weight of 6.61 kg. Upon each impact event, the sensor (which is attached to the impactor) records the contact force and time. By the use of ASTM D7136, the displacement and absorbed energy would be calculated. In addition, for comparing the non-impacted (rear) side of the laminates after each impact event, a high-speed camera is put under the laminates.

3. Results and discussion

3.1. LVI response of thermoplastic laminates

The experimental results regarding the low-velocity impact (LVI) characteristics of thermoplastic (TP) Elium®-based fiber-reinforced polymer composite (FRPC) laminates are demonstrated through Fig. 1 to Fig. 4. Fig. 1 presents the force-time response of the TP laminates with different fiber types and stacking sequences. Fig. 1 (a) shows the force-time behavior for the TP carbon-based laminate (1E) and demonstrates that the contact force goes up until obtaining the maximum load (L_m). Afterward, the laminate cannot tolerate further load, and as a consequence, the load drops and the laminate undergoes damage. Such damage can be distinguished by two regimes, namely subcritical or supercritical. Fig. 1 (a) illustrates that, at all the impact energy levels, after reaching the maximum load (L_m), a massive drop in the force-time curves is observed, which is related to massive delamination and fiber breakage in the laminate (1E). That kind of damage is considered supercritical [16]. In supercritical impact, the impact energy is beyond the damage threshold of the composite laminate. Such damage/failure occurs through several mechanisms, such as matrix cracks, delamination, fiber-matrix debonding, and fiber breakage/fracture [17]. After a massive drop in the load, loss of contact between the structure and the impactor happens. In other words, when the composite laminate is hit by the impactor in a supercritical impact event, some of the back laminas undergo massive delamination. That delamination causes the loss of contact between the impactor and the laminate, resulting in a sudden drop in the force-time (or force-displacement) curve. In Fig. 1(b and c), the force-time behavior of hybrid FRPC laminates at different energy levels is illustrated. At 10 J, some small oscillations can be observed in the behavior of both laminates. At 10 J, after reaching L_m, the damage initiates, resulting in some matrix-cracks; however, the damage is barely visible. High transverse shear stresses generated near the top surface cause those matrix cracks. However, they do not pose a significant threat to structural integrity. However, at 15 J, hybrid laminates 2E and 3E behave differently. Laminate 2E (Fig. 1 (b)) that has carbon layers on the sides suffers from a supercritical impact. However, in laminate 3E that has UHMWPE fabrics on top and bottom, a subcritical impact occurs (Fig. 1 (c)). Surprisingly at 20 J, laminate 3E (Fig. 1 (c)) still shows subcritical impact, while laminate 2E undergoes a supercritical regime. Thus, the hybrid laminate with ductile (UHMWPE) fibers on the sides demonstrates better impact performance [18]. At 33 J, both hybrid laminates suffer from supercritical regimes and perforate. By comparing the maximum contact forces between laminates 2E and 3E at different energy levels, it is noticed that laminate 2E shows higher contact forces compared to those of laminate 3E, Fig. 1(b and c). This is related to the presence of carbon fibers on the sides of laminate 2E, which makes the laminate more brittle; thus, resulting in a higher contact force. As UHMWPE-based laminates can absorb more energy through global deformation, they carry a lower amount of load. The values of maximum contact force (L_m) for different TP laminates at 15 J and 20 J are presented in Table 2 and Table 3, respectively. Fig. 1 (d) illustrates the contact force versus time behavior for laminate 4E. At 15 J, the structure shows a sinusoidal response, where no spike in the behavior is detected. At 20 J, elastic waves generated in the laminate result in some peaks.

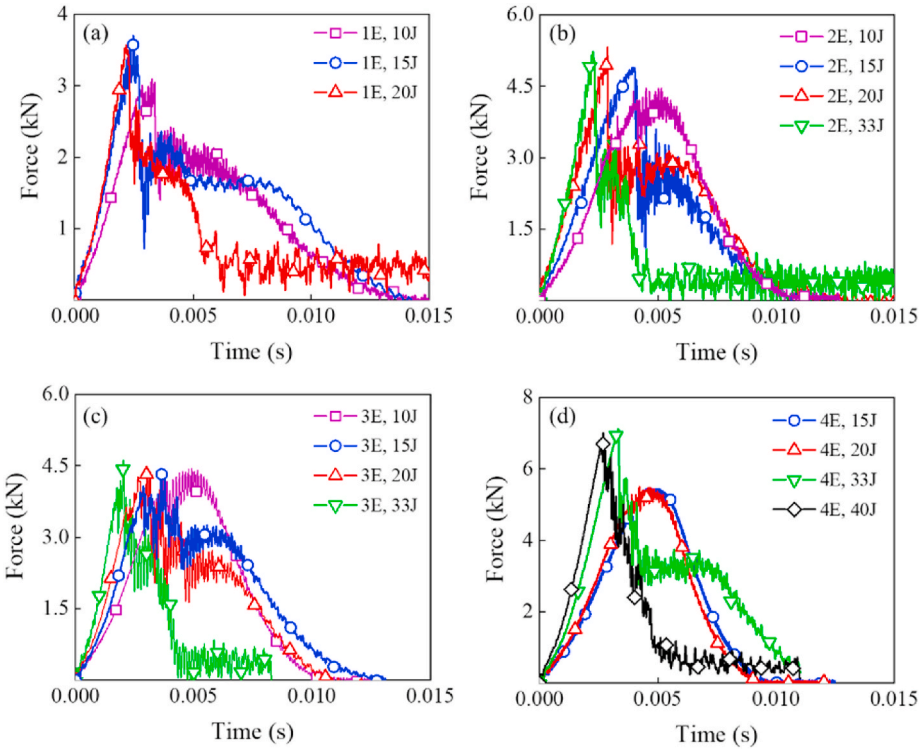

Fig. 1. Contact force versus time curves of thermoplastic FRPC laminates 1E (a), 2E (b), 3E (c), and 4E (d) impacted at various energy levels.

Table 2
Maximum contact force, deflections, structural integrity, and energy parameters for thermoplastic FRPCs impacted at 15 J

Properties	1E: $(Cf)_8$	2E: $(Cf/PEf)_{2S}$	3E: $(PEf/Cf)_{2S}$	4E: $(PEf)_8$	5E: $(Cf)_{14}$
L_m (kN)	3.8 ± 0.1	5.1 ± 0.1	4.7 ± 0.1	5.4 ± 0.1	6.1 ± 0.1
PD_m (mm)	3.6 ± 0.1	7.0 ± 0.2	7.1 ± 0.2	10.6 ± 0.1	6.3 ± 0.2
PD_u (mm)	5.4 ± 0.1	7.7 ± 0.2	7.6 ± 0.1	10.9 ± 0.6	7.3 ± 0.2
PD_u-PD_m (mm)	1.8 ± 0.1	0.7 ± 0.1	0.5 ± 0.1	0.3 ± 0.1	1.0 ± 0.1
E_p (J)	15.6 ± 0.1	15.6 ± 0.1	15.7 ± 0.1	15.7 ± 0.1	15.6 ± 0.1
E_{el} (J)	2.7 ± 0.3	6.3 ± 0.4	6.6 ± 0.1	8.5 ± 0.4	8.3 ± 0.4
E_{ab} (J)	12.9 ± 0.2	9.3 ± 0.8	9.1 ± 0.2	7.3 ± 0.3	7.3 ± 0.2
E_{bml} (J)	8.1 ± 0.2	12.7 ± 0.3	13.9 ± 0.3	15.4 ± 0.3	14.6 ± 0.9
E_{aml} (J)	7.5 ± 0.1	2.9 ± 0.2	1.8 ± 0.1	0.3 ± 0.1	1.0 ± 0.1

Table 3
Maximum contact force, deflections, structural integrity, and energy parameters for thermoplastic FRPCs impacted at 20 J.

Properties	1E: $(Cf)_8$	2E: $(Cf/PEf)_{2S}$	3E: $(PEf/Cf)_{2S}$	4E: $(PEf)_8$	5E: $(Cf)_{14}$
L_m (kN)	3.4 ± 0.2	4.6 ± 0.1	4.9 ± 0.3	5.5 ± 0.1	6.2 ± 0.1
PD_m (mm)	3.2 ± 0.1	5.4 ± 0.2	6.2 ± 0.4	9.9 ± 0.3	4.8 ± 0.3
PD_u (mm)	6.2 ± 0.2	7.6 ± 0.2	7.7 ± 0.2	10.9 ± 0.6	7.5 ± 0.2
PD_u-PD_m (mm)	3.1 ± 0.3	2.2 ± 0.1	1.5 ± 0.1	1.1 ± 0.1	2.6 ± 0.1
E_p (J)	15.7 ± 0.4	19.7 ± 0.1	19.7 ± 0.1	19.7 ± 0.1	19.7 ± 0.1
E_{el} (J)	0.1 ± 0.1	2.5 ± 0.3	5.2 ± 0.2	8.6 ± 0.2	8.6 ± 0.2
E_{ab} (J)	15.6 ± 0.4	17.2 ± 0.8	14.5 ± 0.4	11.1 ± 0.7	11.2 ± 0.7
E_{bml} (J)	7.1 ± 0.3	11.4 ± 0.3	14.2 ± 0.4	17.8 ± 0.8	12.9 ± 0.4
E_{aml} (J)	8.8 ± 0.1	8.2 ± 0.2	5.5 ± 0.2	2.1 ± 0.1	6.8 ± 0.2

However, those peaks do not cause any significant damage (except some matrix crack). Nonetheless, at 33 J and 40 J, supercritical impact occurs. 33 J impact energy level results in partial penetration of laminate 4E; but, at 40 J, the laminate perforates. Fig. 1 (d) demonstrates that, as the impact energy level goes higher, the time to the peak load (L_m) decreases. During a supercritical impact, two scenarios can happen. In the first one, after a massive drop in the load, then the contact force increases again. This is due to the fact that the load would be redistributed to the rear intact plies, which results in the rebound of the impactor (33 J, Fig. 1 (d)). In the second scenario, after obtaining the L_m, the force suddenly drops to (near) zero, followed by many large oscillations, which denotes perforation (40 J, Fig. 1 (d)).

Fig. 2 illustrates the force-displacement behavior of Elium®-based FRPC laminates. LVI force-displacement plots produce remarkable information regarding: the displacement of the laminate at maximum contact load (denoted by PD_m), overall displacement (or deflection) of the laminate (denoted by PD_u), laminate dynamic modulus (the slope of the curve), and the structural integrity index, shown by $PD_u - PD_m$ [16]. The $PD_u - PD_m$ index can provide information concerning the integrity loss in a FRPC structure, and in this regard, higher values indicate a higher loss [16]. Fig. 2(a–d) images show the force-displacement curves for TP laminates 1E to 4E. The enclosed curves indicate that the impactor has rebounded after striking the laminate. However, the open curves show that the impactor has perforated the laminate. The initial part of the force-displacement curve (before reaching L_m) represents the undamaged laminate stiffness. Tables 2 and 3 values present that, from 15 J to 20 J, the displacement at maximum load (PD_m) decreases; however, the overall deflection (PD_u) increases. As the impact energy goes higher, the value of the structural integrity index ($PD_u - PD_m$) increases, confirming a higher loss in integrity. For instance, by increasing the energy level from 15 J to 20 J, laminate 1E loses its integrity by 42% (refer to Tables 2 and 3). At 20 J, the structural integrity value for laminate 2E is measured 2.2 mm, while the value is calculated 1.5 mm for laminate 3E, which shows a higher loss of integrity by 47% (Table 3).

Energy attributes of TP FRPCs at various energy levels are presented in Fig. 3, Table 2, and Table 3. In this regard, peak energy (denoted by E_P) is defined as the amount of the impactor (kinematic) energy transferred to the laminate. In an impact event, three scenarios can happen, namely rebounding, penetration, and perforation. In rebounding, the energy of the impactor is lower compared to the damage threshold of the structure. In that situation, the impact energy curve initially increases until reaching the peak energy (E_P); then, it decreases and obtains a plateau trend, which is known as absorbed energy (denoted by E_{ab}).

For instance, laminate 1E at 10 J, shows rebounding (Fig. 3 (a)). Absorbed energy mainly is used to generate various damage modes. In the case of a TP or a toughened TS matrix, plastic deformation can also be considered as another damage mode. When the impactor rebounds, the energy kept temporally in the laminate would be transferred to the impactor again, which is called elastic energy (denoted by E_{el}). If the impact energy increases beyond the damage threshold of the structure, the laminate penetrates. In this scenario, the energy-time profile, after reaching peak energy, does not increase or decrease, rather it gets a constant trend. By a further increase in the energy level, perforation happens. In perforation, after reaching peak energy, the energy-time curve increases at a constant rate. Laminates 2E and 3E at 33 J exhibit perforation (Fig. 3 (a)). Another important energy parameter for analyzing the response of a FRPC laminate under LVI is called major damage energy (denoted by E_{bml}). Major damage energy is the energy corresponding to the maximum contact force. In other words, the energy absorbed by the laminate before happening the significant damage is called major damage energy [16]. As a result, a higher value of E_{bml} (compared to a specific impact energy level) demonstrates a lower extent of damage in that structure. The amount of absorbed energy after the occurrence of the significant damage is shown by E_{aml}.

The equation of $E_p = E_{bml} + E_{aml}$ can be used to calculate the amount of absorbed energy after the incident of significant damage. The values of major damage energy for TP FRPCs impacted at 15 J and 20 J are tabulated in Tables 2 and 3, respectively. By comparing the absorbed energy values of hybrid laminates, it is noticed that, at 15 J and 20 J, laminate 2E absorbs less energy compared to laminate 3E, indicating a lower extent of damage and integrity loss.

3.2. The influence of fiber type

To evaluate the influence of the fiber type and compare the LVI characteristics of carbon-based and UHMWPE-based TP FRPC laminates with the same thickness, the force-time, force-displacement, and energy-time curves at different energy levels are provided in Fig. 4. The contact force-time curves at energy levels of 15 J and 20 J show that (carbon-based) laminate 5E demonstrates higher values regarding maximum contact force by 11% compared to those of (UHMWPE-based) laminate 4E (Fig. 4 (a)). That difference is related to tensile and shear properties as well as failure modes of each laminate's fiber type. At 15 J, laminate 4E does not show any damage; however, laminate 5E exhibits a lot of peaks, followed by a small drop load (subcritical regime). By comparing the force-displacement curves, it is noticed that the value of the structural integrity index for laminate 5E is higher by 233% compared to that of laminate 4E, which shows a significantly higher loss in laminate 5E integrity, Fig. 4 (b). By comparing the slopes of the force-displacement curves, (the dynamic modulus of) laminate 5E shows higher values compared to those of laminate 4E. Due to the ductile behavior of UHMWPE fibers, both the displacements at maximum load and overall

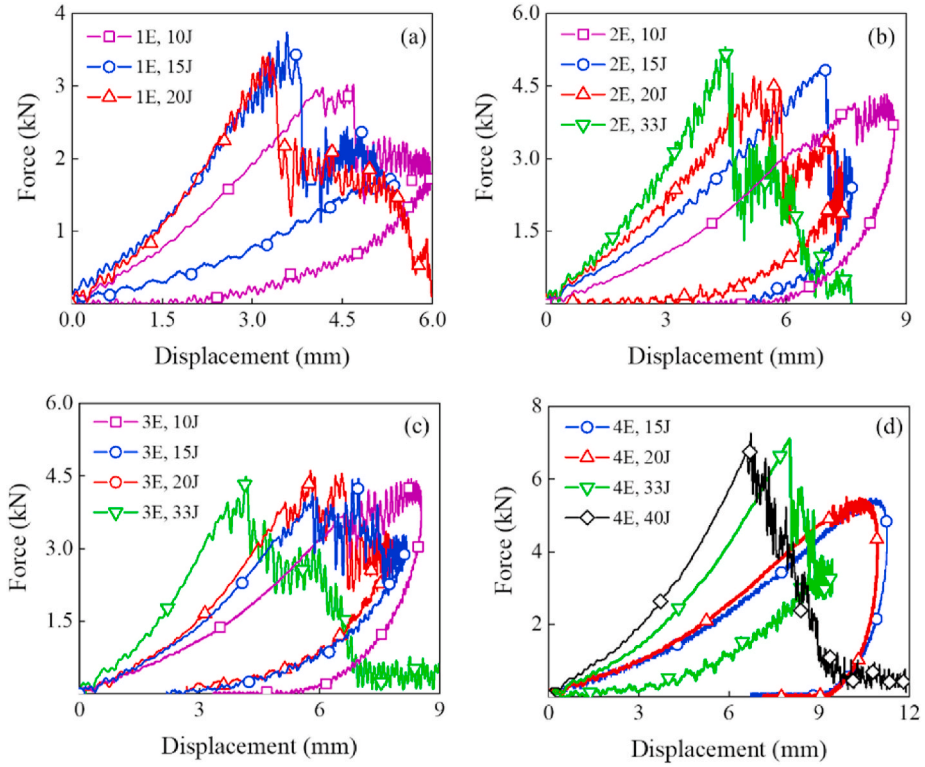

Fig. 2. Contact force versus displacement curves of thermoplastic FRPC laminates 1E (a), 2E (b), 3E (c), and 4E (d) impacted at various energy levels.

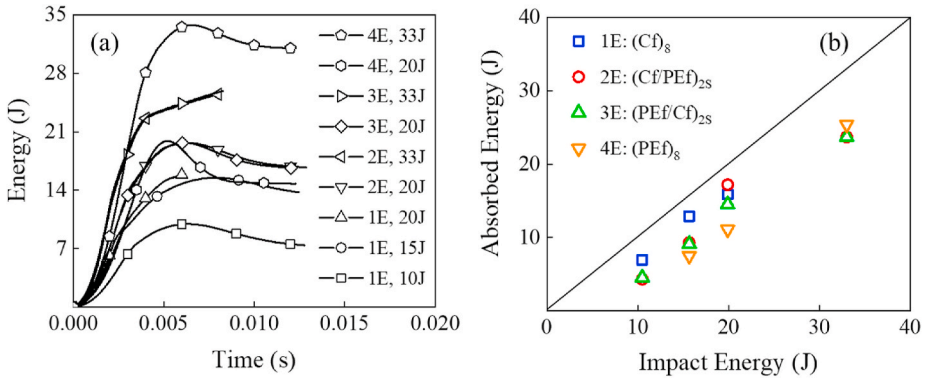

Fig. 3. Energy versus time curves (a) and absorbed energy versus impact energy values (b) of thermoplastic laminates impacted at various energy levels.

deflection for laminate 4E are much higher than those of laminate 5E. Concerning energy attributes, although at 15 J and 20 J both the laminates absorb almost the same amount of energy, laminate 5E shows higher values of E_{aml} by 233% at 15 J, and 220% at 20 J compared to those of laminate 4E. This confirms that the extent of damage after the occurrence of major damage energy in carbon-based structures is remarkably greater than that of the UHMWPE-based counterpart. At 33 J, laminate 5E perforates; however, the impactor rebounds when it strikes laminate 4E, Fig. 4(b and c).

3.3. The influence of resin type and stacking sequence

The force-time, force-displacement, and energy attributes regarding the influence of stacking sequence and resin type on the LVI behaviors of TP and TS FRPC laminates are presented through Fig. 5 to Fig. 7 as well as Table 4. The laminates are fabricated with Elium® (Fig. 5 (a1-a2)), Epolam (Fig. 5 (b1-b2), and Sikafloor® (Fig. 5 (c1-c2) resins and tested at 15 J and 20 J. By comparing the force-time response at 15 J (Fig. 5 (a1-b1-c1)) and 20 J (Fig. 5 (a2-b2-c2)), it is observed that, at 15 J, laminate 4E shows a sinusoidal trend without any spike or oscillation, while a partial sinusoidal trend with many oscillations has occurred for the TS counterparts (i.e. laminates 4P and 4S). As a result, the TP laminates show better impact resistance performance with regards to the TS laminates. Concerning the force-time behavior of hybrid FRPC laminates at 15 J, all three hybrid laminates 2E, 2P, and 2S undergo supercritical impact. However, laminates 3E, 3P, and 3S undergo subcritical impact. This demonstrates that, irrespective of the matrix type, the laminates with ductile (UHMWPE) fabrics on top and bottom show better impact performance compared to laminates with brittle (carbon) fabrics on the sides. The comparison of the structural integrity index values (PD_u – PD_m, provided in Table 4) demonstrates that the TP laminates enjoy lower values compared to those exhibited by the TS counterparts. Besides, the value of PD_m is higher for the TP laminate, which is related to a higher elastic/plastic deflection offered by the TP laminate until the maximum load is achieved [16].

Fig. 6 shows the force-displacement response of thermoplastic and

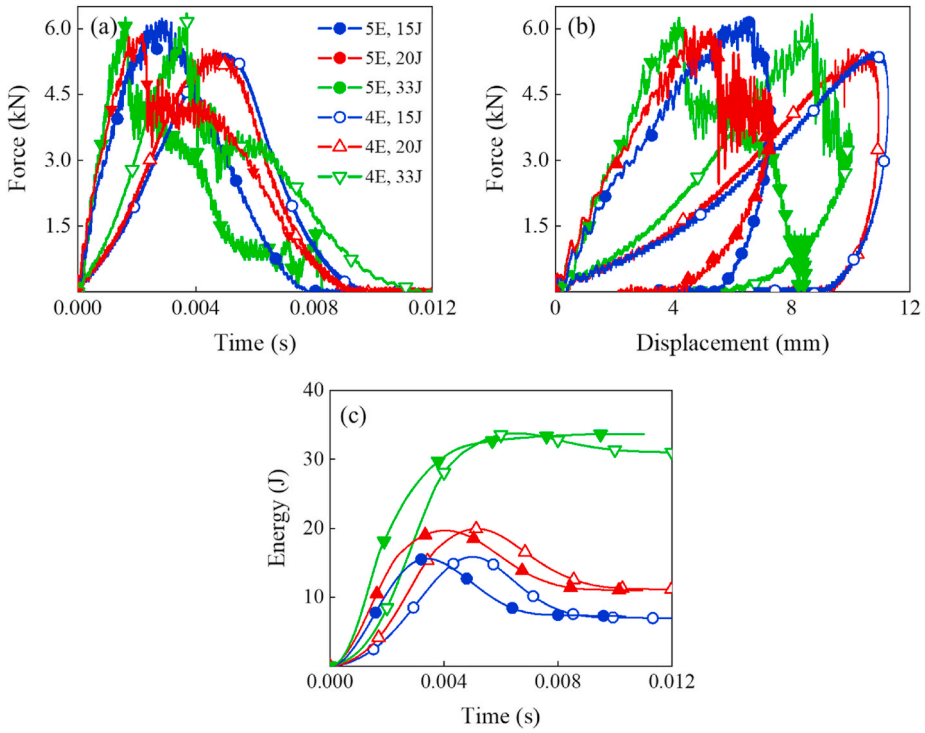

Fig. 4. The comparison of force-time (a), force-displacement (b), and energy-time (c) curves for thermoplastic laminates with different fiber types at various energy levels.

thermosetting composites impacted at energy levels of 15 J and 20 J. Fig. 6 (a1-b1-c1) show that the dynamic modulus for carbon-based laminates (that are 1E, 1P, and 1S) is greater than that of the UHMWPE-based counterparts (that are 4E, 4P, and 4S). The stiffness values of the hybrid laminates are greater than those of UHMWPE-based and smaller than those of carbon-based FRPC laminates. However, by using the same number of fabrics with different stacking sequences, it is observed that there is a subtle difference in dynamic moduli between the hybrid group laminates 2 and 3. Fig. 6 (a1-b1-c1) show that group laminates 2 (that contains carbon fibers on the top and bottom) exhibits a bit greater dynamic modulus compared to that of group laminates 3 (which have UHMWPE fibers on the sides). As the LVI response is significantly governed by the behavior of the fibers at the rear side of a laminate, group laminates 2 demonstrates a higher dynamic modulus compared to that of laminates group 3. This difference is related to the tensile and shear properties as well as failure modes of each laminate's fibers, which show higher values and brittle characteristics for carbon fibers. Fig. 6 (a2-b2-c2) demonstrate that irrespective of the resin type and impact energy level, such behavior exists in the LVI response of the hybrid laminates. Regarding the influence of the resin, force-displacement behavior at 15 J (Fig. 6 (a1-b1-c1)) shows that the enclosed area is greater for the thermoplastic laminates compared to that of corresponding thermosetting counterparts. Furthermore, by comparing the values of the structural integrity index, $PD_u - PD_m$, the TP laminates enjoy lower values compared to those exhibited by the TS counterparts. Besides, the value of PD_m is higher for the TP laminate, which is related to a higher elastic/plastic deflection offered by the laminate until the maximum load is achieved. This reveals that the TP laminate has more tendency to deform before obtaining the maximum load. At 20 J, more drastic changes in the dynamic modulus in the area between PD_m and PD_u is observed, Fig. 6 (a2-b2-c2). That change represents matrix cracking and fibers failure in a FRPC structure. To quantitatively investigate the effect of resin type on the LVI characteristics of hybrid structures, the difference between the values of the structural integrity index is summarized in Table 4. The values reveal that the TP laminate (3E) has better structural integrity by 100% and 20% compared to that of Epolam-based (3P) and Sikafloor®-based (3S) counterparts, respectively.

Fig. 7(a and b) demonstrate the comparison of the structural integrity index values as well as major damage energy values for the laminates with TP and TS resins. For this, laminates 3E, 3P, and 3S are considered as examples, since they enjoy better impact performance compared to the other type of hybrid system (laminate 2E). The permanent deflections are presented in Fig. 7 (a). The TP laminate shows better performance in terms of structural integrity in comparison to that of the thermosetting structures. Fig. 7 (b) presents the values of major damage energy (E_{bml}) for the group laminates 3 with different resins. At various energy levels, laminate 3E enjoys higher values compared to those presented by laminates 3S and 3P. Higher values of E_{bml} demonstrates that remarkable energy is absorbed via elastic-plastic deformations before the beginning of the significant damage (E_{aml}) [12].

3.4. Failure modes analysis

FRPCs can absorb energy through various means, namely indentation (matrix cracking and/or local fiber failure/breakage), delamination (inter-yarn failure), splitting (fiber breakage/failure) or fibers peeling on the rear side [19]. As mentioned earlier, during an impact event three scenarios can occur, namely rebounding (with/out delamination), penetration, and perforation. In rebounding and low energy levels, the impact energy is (much) lower than the damage threshold of the structure, and the absorbed energy mainly does not cause remarkable damage (except matrix cracking and indentation). By increasing the impact energy (to near the damage threshold of the structure), significant delamination occurs. As indentation grows, the matrix under the impactor crushes, and therefore, delamination in the FRPC laminate interfaces propagates remarkably, which is due to bending-induced stresses. In the case of a TP or a toughened TS matrix, plastic deformation can also be considered as another failure mechanism. If the impact energy increases further to reach the damage threshold of the structure, the laminate penetrates; as a result, all the layers in the laminate are delaminated around the impact zone. In penetration, the whole energy

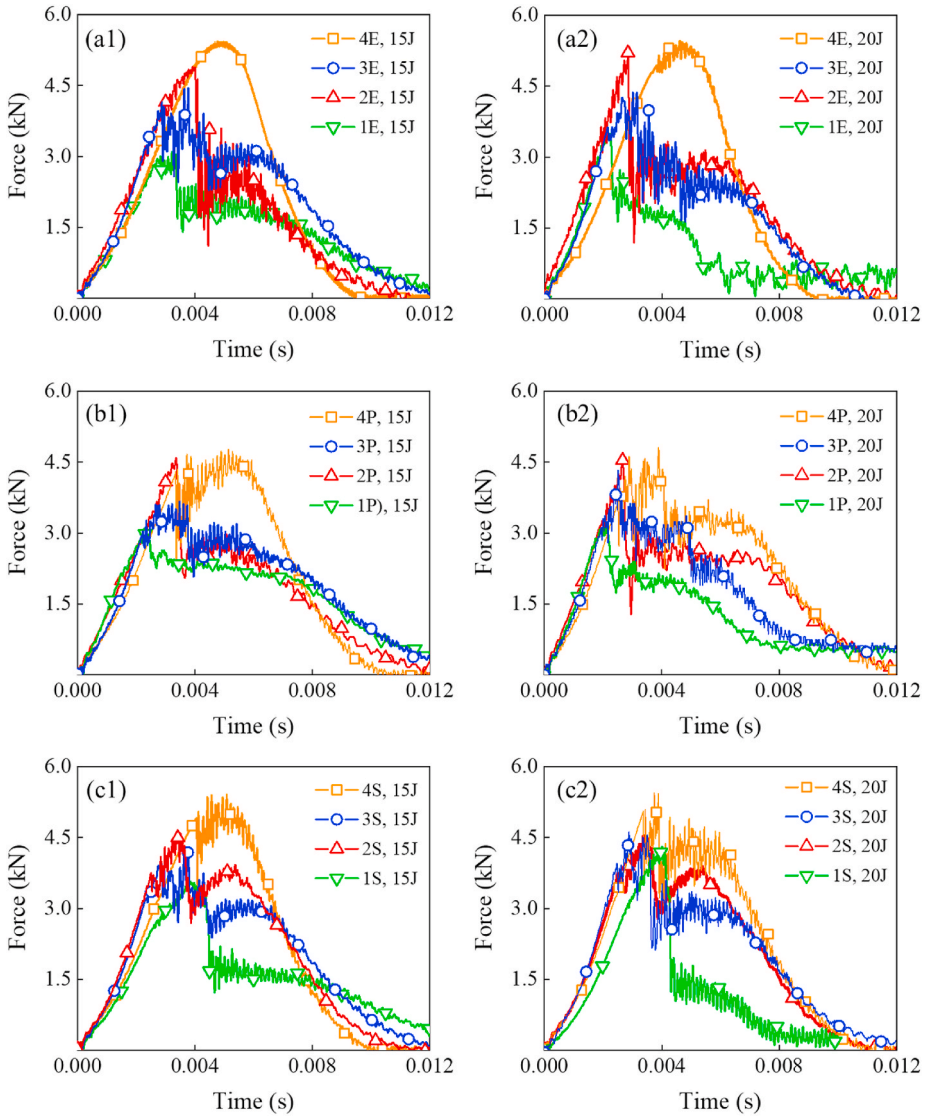

Fig. 5. Force-time behaviors of Eium®-based (a1-a2), Epolam-based (b1-b2), and Sikafloor®-based (c1-c2) FRPCs impacted at energy levels of 15 J and 20 J.

Table 4
Maximum contact force, deflections, structural integrity, and energy parameters for laminates 3E, 3P, and 3S at the energy level of 20 J.

Properties	3E: $(PEf/Cf)_{2S}$	3P: $(PEf/Cf)_{2S}$	3S: $(PEf/Cf)_{2S}$
L_m (kN)	4.9 ± 0.3	4.3 ± 0.2	4.5 ± 0.3
PD_m (mm)	6.2 ± 0.4	5.2 ± 0.4	6.2 ± 0.3
PD_u (mm)	7.7 ± 0.2	8.2 ± 0.2	8.0 ± 0.2
PD_u-PD_m (mm)	1.5 ± 0.1	3.0 ± 0.1	1.8 ± 0.2
E_p (J)	19.7 ± 0.1	19.7 ± 0.1	19.7 ± 0.1
E_{el} (J)	7.4 ± 0.2	1.5 ± 0.1	5.1 ± 0.2
E_{ab} (J)	12.3 ± 0.4	18.2 ± 0.7	14.6 ± 0.5
E_{bml} (J)	13.9 ± 0.4	10.3 ± 0.5	12.9 ± 0.4
E_{aml} (J)	5.8 ± 0.2	9.4 ± 0.3	6.8 ± 0.2

of the impactor transfers to the laminate, and the impactor (after penetrating the last lamina) stops. In this situation, for the first time, the absorbed energy reaches the level of the impact energy [20]. The major forms of energy absorption during penetration are shear out, delamination, and elastic flexure [21]. By a further increase in the energy level, perforation happens. In perforation, the impactor perforates the laminate completely and comes out from the rear side of the structure. Fig. 8 provides the non-impacted side images of Elium®-based laminates (1E to 4E) impacted at 15 J (a-d) and 20 J (e-h). At 15 J, carbon-based laminate (1E) penetrates partially. Fig. 8 (a) shows that the first failure mode is visible matrix cracks, running in the inclined 45° directions. The size of cracks and damage along the two directions is a bit larger than that of the diameter of the impactor. The hybrid laminates (2E and 3E) do not penetrate or perforate in contrast to laminate 1E, rather the impactor rebounds after that impact event. In hybrid laminates, matrix cracking and delamination are expected as failure mechanisms, Fig. 8(b and c). However, there is a difference in terms of the rear side damage of hybrid laminates. Since UHMWPE fibers enjoy higher strain to failure in tension, the splitting of the back face does not happen in laminate 3E (in contrast to laminate 2E). As a result, larger delamination occurs in laminate 2E. UHMWPE-based laminate (4E) undergoes a small amount of plastic deformation without suffering any damage, Fig. 8 (d). At 20 J, laminate 1E perforates (Fig. 8 (e)); laminates 2E and 3E (Fig. 8(f and g)) suffer from a greater extent of damage and delamination compared to those at 15 J. However, laminate 4E undergoes a small amount of matrix cracking and plastic deformation, Fig. 8 (h). In contrast to carbon-based laminates, which are locally deformed, laminate 4E shows global deformation and exhibits a bulge at the rear side.

Fig. 9 images illustrate the difference between the cross-sectional behaviors of the hybrid structures impacted at different energy levels. By comparing the response of the structures at 15 J (Fig. 9 (a1-b1)), it is noticed that the extent of damage size is almost similar. However, the

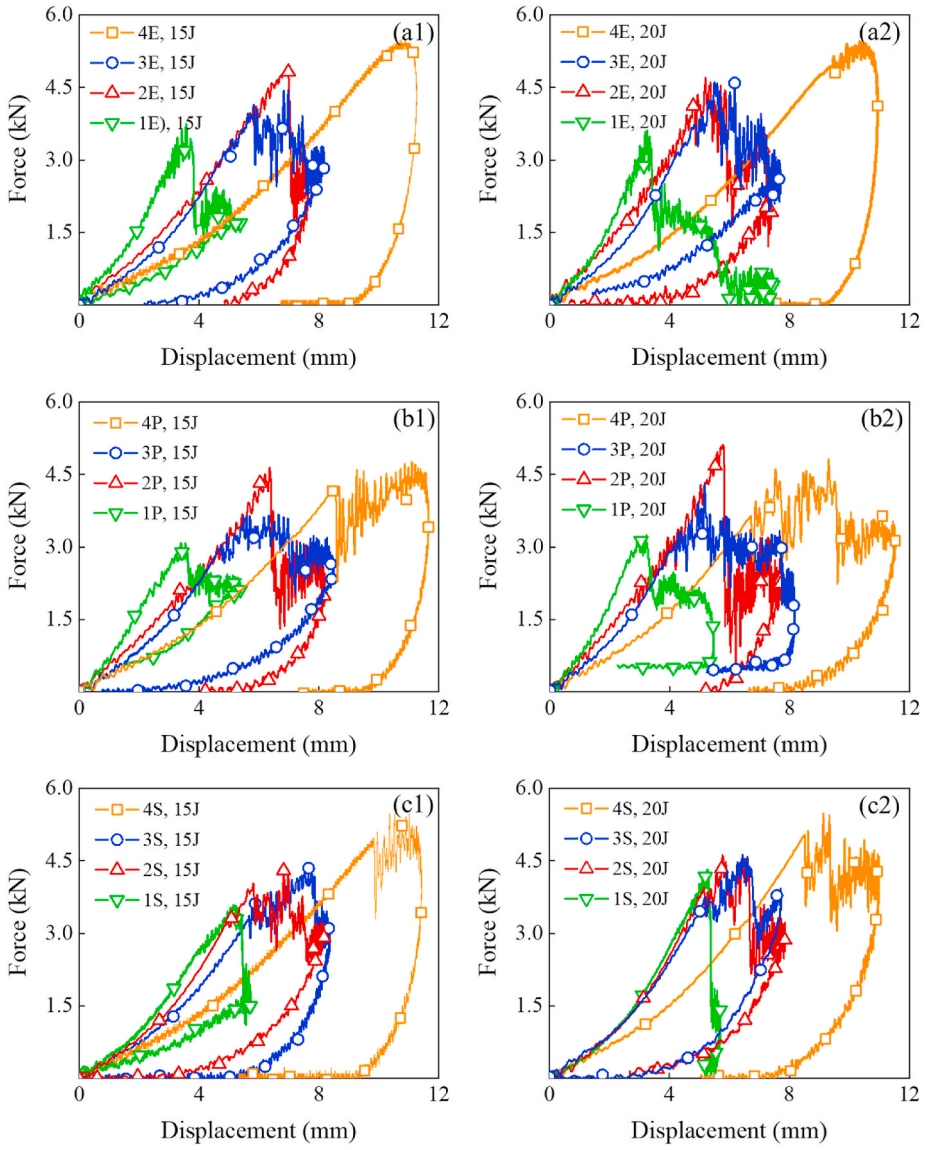

Fig. 6. Force-displacement behaviors of Eium®-based (a1-a2), Epolam-based (b1-b2), and Sikafloor®-based (c1-c2) FRPCs impacted at 15 J and 20 J.

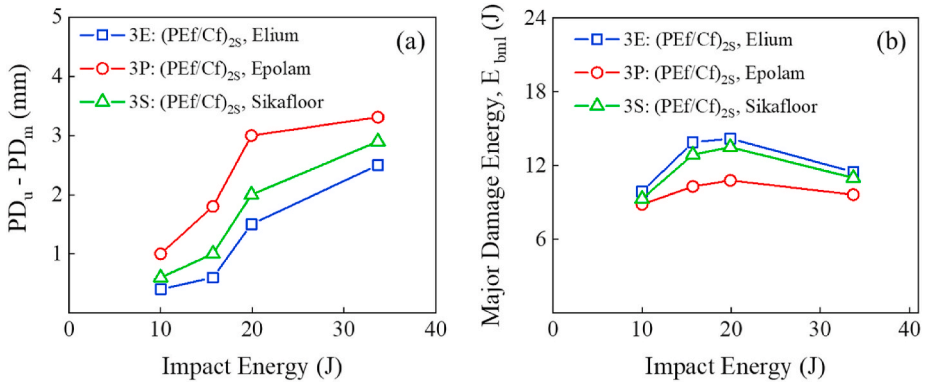

Fig. 7. The comparison of structural integrity (a), and major damage energy (b) values of impacted thermosetting and thermoplastic laminates at different energy levels.

top and bottom plies of laminate 2E exhibit a smaller amount of deformation compared to that of laminate 3E, which is related to the presence of brittle carbon fibers. At 20 J (Fig. 9 (a2-b2)), interlaminar cracks and fibers breakage are more obvious within the laminates. At 33 J (Fig. 9 (a3-b3)), due to the presence of carbon fabric at the rear side, catastrophic failure and delamination are observed, which are followed by

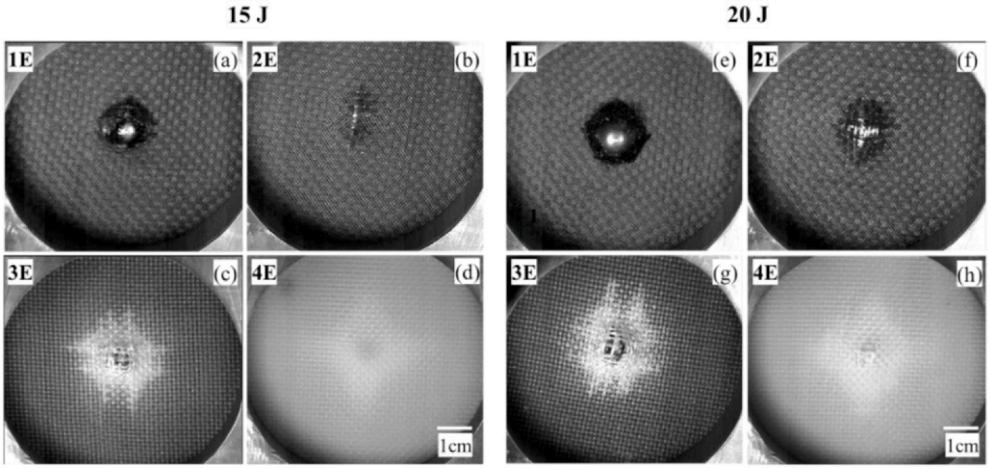

Fig. 8. Images of the rear side of the TP laminates impacted at energy levels of 15 J (a–d) and 20 J (e–h).

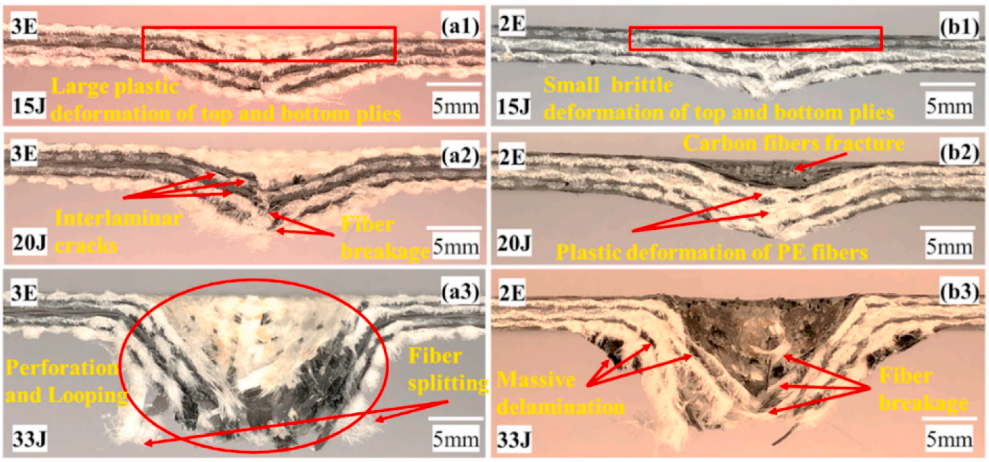

Fig. 9. The cross-sectional images of hybrid laminates 3E (a1-a3) and E2 (b1-b3) impacted at 15 J, 20 J, and 33J

the splitting of the fabric fibers. However, thanks to the presence of ductile UHMWPE fibers and their ability to stretch in tension, the laminate 3E suffers less damage compared to laminate 2E. Fig. 10 shows the morphological characterizations of different thermoplastic laminates impacted at different energy levels. Fig. 10 (a) shows the matrix cracking, delamination, and partial debonding in the carbon-based laminate (1E) impacted at 10 J. As can be observed, the initiation and propagation of the cracks in the bottom layers are more obvious, since the cracks in thin FRP laminates (here 1E) initiate in the lower plies and then propagate towards the upper plies. Some of the cracks propagated, resulting in partial debonding between the adjacent layers and delamination. However, by introducing UHMWPE fibers to the laminate and making a hybrid system, the initiation and propagation of the cracks suppress significantly as illustrated in Fig. 10 (b), which shows the side view of the hybrid laminate 2E impacted at 10 J. The behavior of different fiber types after significant damage is illustrated in Fig. 10(c and d); which shows a brittle failure for carbon fibers (Fig. 10 (c)) and a ductile failure for UHMWPE fibers (Fig. 10 (d)).

Besides, it can be observed that, at the end of an impact event, UHMWPE fibers are significantly elongated (with necking), while carbon fibers lack such a characteristic. The ductile response of UHMWPE fibers denotes that the energy absorption capability of UHMWPE-based laminates is much higher than that of the carbon-based counterparts. The back face images of the impacted laminates 4E and 5E (which have the same thickness) are presented in Fig. 11. In lower impact energy levels, namely 15 J (Fig. 11 (a1-b1)) and 20 J (Fig. 11 (a2-b2)) both laminates behave (almost) similarly, although the nature of local and global deformations differs for two laminates. By increasing the impact energy to 27 J (Fig. 11 (a3-b3)) and 33 J (Fig. 11 (a4-b4)), the laminates exhibit different responses. At 27 J, laminate 5E penetrates, Fig. 11 (b3); however, the impactor rebounds when it strikes laminate 4E, Fig. 11 (a3). Nevertheless, at 33 J, laminate 5E perforates and massive delamination occurs, while laminate 4E still shows rebounding.

The role of resin type on the LVI characteristics of composites is demonstrated in cross-sectional images provided in Fig. 12. The TP laminate (1E) and TS counterparts (1P and 1S) are impacted at 20 J, which resulted in perforation. However, the TS laminates show small brittle deformation (Fig. 12(b and c)), while the TP laminate has experienced large plastic deformation (Fig. 12 (a)). This advantage in the TP structure is due to the higher fracture toughness of the Elium® resin [22]. Failure analysis on impacted laminates shows that the TS laminates undergo elastic deformation, delamination, surface buckling, fibers shear-out, and fibers fracture. However, plastic deformation is considered as an extra failure mechanism for the TP counterpart. The ductile TP resin slows the propagation of micro-cracks and the voids within the plastic crack zone, because the damage happens by cavitation, resulting in inducing matrix shear banding [23]. However, TS FRPC structures lack such an advantage, and as a result, catastrophic brittle failure happens. It can be inferred that thermoplastic resin plasticization plays a remarkable influence in the response of TP structures.

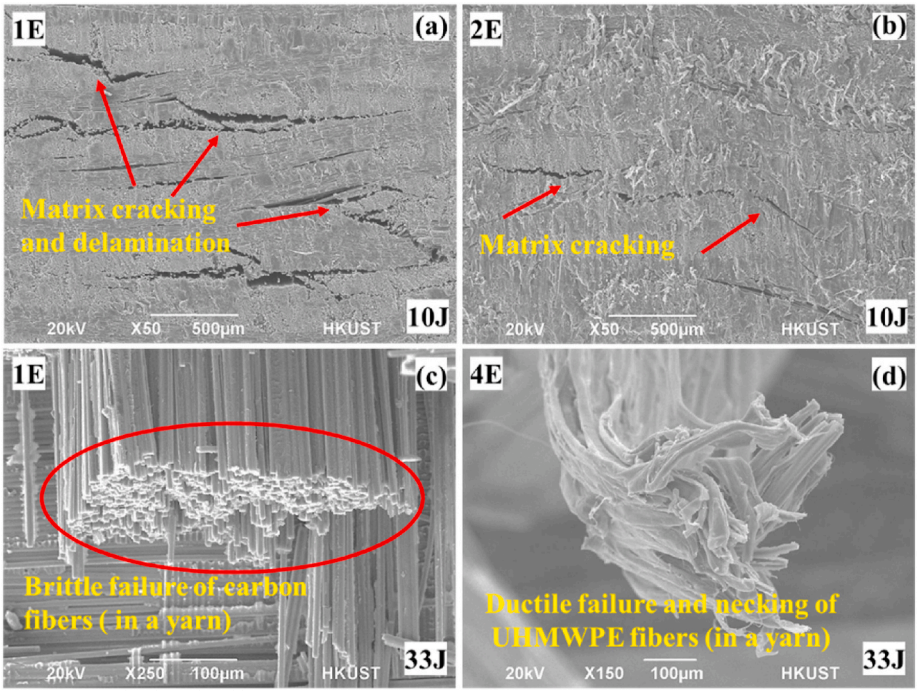

Fig. 10. Microscopic observations of matrix cracking, delamination, and debonding in laminate 1E (a) and 2E (b) impacted at 10 J; the failure of (laminate 1E) carbon fibers (c) and (laminate 4E) UHMWPE fibers (d) at 33 J.

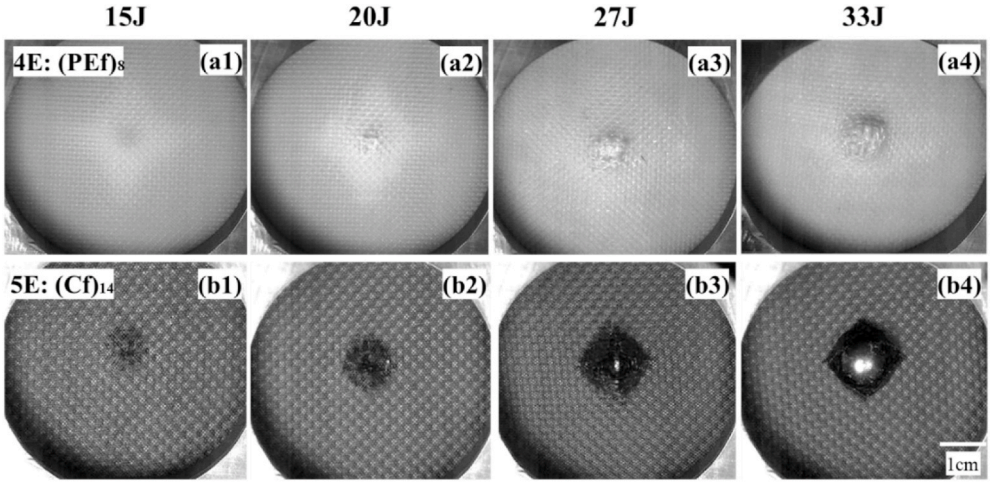

Fig. 11. Images of the non-impacted (rear) side of laminate 4E (a1-a4) and laminate 5E (b1-b4) at different impact energy levels.

3.5. Numerical simulations

3.5.1. Modeling

To verify the experimental results and also evaluate the relevance of the mechanics of the structure genome (MSG) developed in the previous studies for the LVI applications [14,15,24], LVI simulations are performed on the carbon-based FRPC laminate (1E). In this regard, a damage model is introduced via a user-defined material code (VUMAT) in ABAQUS/Explicit to simulate the interlaminar failure (delamination), and intralaminar failures, including fiber tensile or compressive failure, matrix tensile or compressive failure, and the damage in the fiber-matrix interface. To define the elastic properties of laminate 1E in ABAQUS/Explicit, the material properties needed, which are obtained by the MSG as well as experiments in the previous studies [13,14] and are provided in Table 5 and Table 6. Damage under shear loading and plastic deformation are considered to capture the matrix dominated shear response of a ply [25]. Some of the damage initiation values are already calculated by the experiments in the previous study [13], including: ultimate tensile strength in the warp (X_{1+}) and weft (X_{2+}) directions, ultimate compressive strengths in the warp (X_{1-}) and weft (X_{2-}) directions, and ultimate in-plane shear strength (S_{12}). The damage growth results from critical energy criteria [26]. The values are obtained through the fiber directions in tensile ($G^{1+} = G^{2+}$) and compression ($G^{1-} = G^{2-}$). Johnson et al. [27] described the parameters of α_{12} (in the equation of shear damage), and d_{12}^{max} (maximum shear damage) to further model the damage growth. Due to the reason that the procedure in determining the values of the fracture energies (described in Pinho et al. [28]) is complex, the values are obtained as proposed by Schwab et al. [25]. The (plastic) non-linear response of the woven plies caused by the intra-laminar damage may be modeled by the pseudo-plastic law. The shear plasticity behavior can be obtained by using Eq. (1),

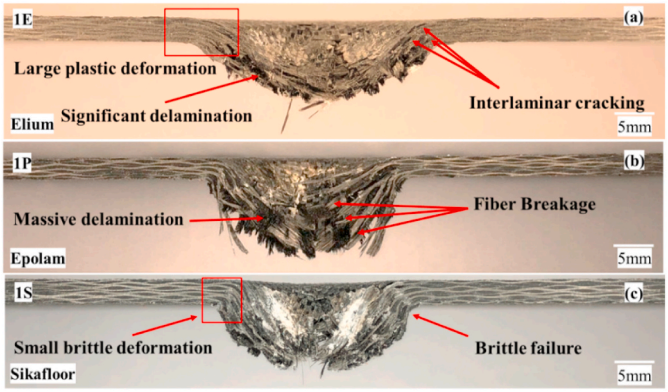

Fig. 12. The comparison of cross-sectional observations of the carbon-based thermoplastic (a) and thermosetting (b, c) laminates at 20 J.

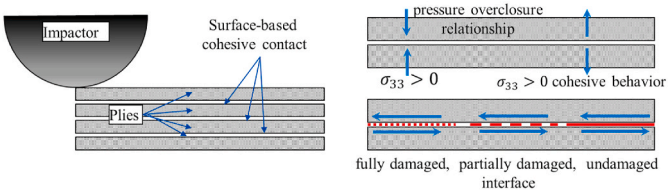

Fig. 13. Schematic of load transfer behavior of surface-bashed cohesive contact method [32].

Table 5
Material characteristics describing the elastic behavior of the carbon fabric/Elium® lamina [13,14].

Elastic constants	$E_1^+ = E_2^+$	$E_1^- = E_2^-$	G_{12}	$\upsilon_{12}^+ = \upsilon_{12}^-$
	57.3 GPa	57.3 GPa	5.1 GPa	0.052

$$\tilde{\sigma}_0(\tilde{\varepsilon}^{pl}) = \tilde{\sigma}_{y0} + C(\tilde{\varepsilon}^{pl})^p \tag{1}$$

where, $\tilde{\sigma}_{y0}$ is the initial effective shear yield stress, C and p are the coefficient and the power term in the hardening equation, respectively. As the aforementioned continuum damage mechanisms associated with the stiffness degradation, excessive distortions of elements or other numerical difficulties may occur during the simulation. To alleviate such problems, a criterion of element deletion is employed, where an element would be deleted when one of the damage variables for the fiber or matrix in tensile or compression reaches to 0.99 (at one integration point but all associated section points). The material characteristics describing the elastic behavior, damage initiation and evolution, and shear plasticity parameters for laminate 1E are provided through Table 5 to Table 7.

To model the initiation and propagation of delamination, various methods are proposed in the literature. Among different approaches, cohesive zone models that combine the fracture mechanics energy and strength-based damage criteria have attracted considerable attention recently [29–31]. Hence, in this study, the CZM based on traction separation constitutive law is applied. To reduce the computational time significantly, a surface-based cohesive contact method is applied in this study to simulate the initiation and propagation of delamination in the interface between the adjacent plies. The surface-based cohesive contact method permits the specification of generalized traction-separation behavior of two nearby surfaces [32]. This method provides the feasibility of delamination damage modeling, which is close to the cohesive elements that are applied using a traction-separation law. The schematic of the load transfer behavior of the surface-bashed cohesive contact

Table 6
Material characteristics describing the damage initiation and evolution of the carbon fabric/Elium® lamina [13].

Nominal strengths/ crit.	$X_1^+ = X_2^+$	$X_1^- = X_2^-$	S_{12}	$G_f^{1+} = G_f^{2+}$	$G_f^{1-} = G_f^{2-}$
energy release rate	710 MPa	240 MPa	60 MPa	18 MPa	14.5 MPa

Table 7
Shear plasticity equation coefficients and associated damage evolution parameters [25].

parameters	$\tilde{\sigma}_{y0}$	C	P	α_{12}	d_{12}^{max}
	65 MPa	1650 MPa	0.5	0.186	1.0

Table 8
Properties of the surface-bashed cohesive contact method [33].

Elastic properties	E_n = 1370 GPa	G_t = 493 GPa	G_s = 493 GPa
Traction forces	t_n^0 = 62.3 MPa	t_t^0 = 92.3 MPa	t_s^0 = 92.3 MPa
Crit. frac. toughness	$G_{IC} = 0.28\left(\frac{N}{mm}\right)$	$G_{IIC} = 0.79\left(\frac{N}{mm}\right)$	$G_{IIIC} = 0.79\left(\frac{N}{mm}\right)$

method is depicted in Fig. 13 [32]. The CZM adopted in this study has an entirely elastic behavior till the beginning of the damage. The damage initiation principle is proposed by a quadratic function as provided in Eq. (2)

$$\left(\frac{\sigma_n}{N}\right)^2 + \left(\frac{\sigma_t}{T}\right)^2 + \left(\frac{\sigma_s}{S}\right)^2 = 1 \tag{2}$$

where σ_n, σ_t, and σ_s represent the tensile stress in the normal (n) and shear directions (s and t), respectively. N, T and S represent their critical values. The damage growth is predicated under a mixed-mode loading as proposed by Benzeggagh-Kenane (B–K) through the fracture energy law provided in Eq. (3) [26]:

$$G = G_{IC} + (G_{IIC} - G_{IC}) \times \left(\frac{G_{II} + G_{III}}{G}\right)^{\eta} \tag{3}$$

where G_{IC}, G_{IIC}, and G_{IIIC} are the critical energy release rates under mode I, mode II, and mode III, respectively. $G = G_{IC} + G_{IIC} + G_{IIIC}$ is the total energy release rate. η is the B–K parameter, which is estimated from the literature as 1.45 [33]. The relevant material data for the cohesive contact model used in the present study are tabulated in Table 8 [33].

To reproduce the experimental setup used in the impact test, eight layers of carbon FRPC lamina are stacked on top of one another resulting in 1.6 mm nominal thickness and modeled as homogenous orthotropic layers connected by the cohesive zone model. The lamina is considered as a circular plate with a diameter of 76 mm. The edge of the laminate is fully clamped to simulate the experimental boundary conditions. The hemispherical impactor with a diameter of 12 mm and the rigid body of mass 6.61 kg is placed at the top center of the plate. The velocity of the impactor is changed based on the desired impact energy performed in the experimental part. The displacement of the impactor is constrained to move vertically and is placed with a small distance of 0.001 from the plate. The interaction between the impactor and the plate is modeled by surface-to-surface contact pairs with the friction coefficient of 0.3. Besides, a frictionless tangential behavior is considered between the plies. Regarding the mesh size, elements with the size of 0.25 mm × 0.25 mm are considered for the impact zone and courser mesh is adopted in the zone far away from the zone around the impactor. Due to the symmetry

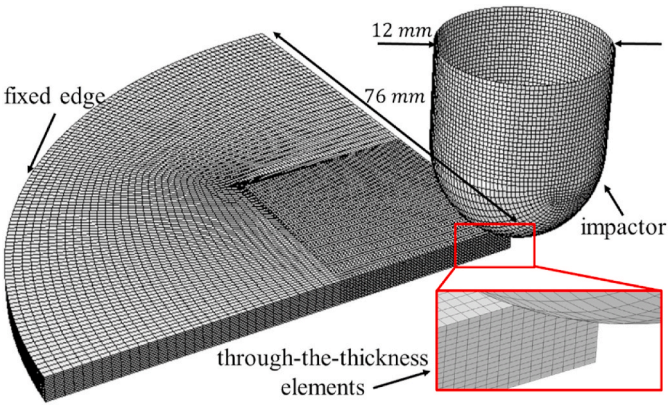

Fig. 14. FE model used for numerical simulation of (a quarter of) laminate 1E under LVI.

in the model, only a quarter of the model is considered, Fig. 14. In the direction of thickness, two elements are considered for each lamina.

3.5.2. Results

The numerical results regarding the force-time, force-displacement, and force-energy curves of the carbon-based FRPC laminate (1E : Cf_8) at 10 J and 20 J are provided in Fig. 15. Fig. 15 (a) compares the experimental and numerical results regarding the load versus time response of laminate 1E. As can be observed, the numerical response is in a good agreement with that of the experimental test. In terms of the predicted maximum load, the difference is less than 1% at 10 J. However, by increasing the impact energy to 20 J, the difference increases, which is related to the material model implemented in the simulation. Besides, the slope of the curve (in the FE model) in the loading and unloading phases matches well with the experimental results. In the loading phase, the load is related to the elastic flexure of the plate until obtaining the maximum load. The time to the peak (load) for the FE model also agrees well with that of the experiment (with less than 1% difference). Nonetheless, at 10 J, the first load drop in the experiment (curve) is small, followed by a partial increase in the load, and finally by a massive drop in the loading. However, the FE model shows just one significant (load) drop in the response, which denotes matrix cracking and delamination in the structure. Fig. 15 (b) demonstrates the comparison of experimental and the FE model force-displacement behaviors of laminate 1E at energy levels of 10 J and 20 J. At 10 J, the slope, at the loading phase (which corresponds to the dynamic modulus of the structures) is simulated accurately. Besides, the displacement at the corresponding first load drop is very close to that obtained by the experiment. The difference between the maximum deflection of the laminate between the FE model and the experiment is less than 3%. The unloading phase in the FE model also matches well in the experiment, which denotes the springback of the plate. However, at 20 J, the results for the experiment and the FE model have some discrepancies. The discrepancies are related to the model and perforation in the structure, which the latter one makes the material behavior complicated, and therefore, the model is less accurate compared to that of lower energy levels, namely 10 J [26]. The energy versus time curves of the experiment and FE model is presented in Fig. 15 (c), which allows us to compare the value of the impact energy and also the amount of absorbed energy by the laminate computationally. As can be observed, the upward and downward slopes of the FE model is very satisfactory compared to those obtained by the experiment at 10 J. In terms of the impact energy, the difference between the FE model and experiment is less than 5%, and more importantly, the difference between the absorbed energy values is less than 0.5%. Fig. 15 (d) shows the tensile damage/failure of warp fibers in laminate 1E, which was obtained by implementing the VUMAT code in Abaqus/Explicit. Fig. 16 demonstrates the back face of the perforated carbon FRPC laminate (1E) at 20 J, which plastic strain repartition at the end of the FE model (Fig. 16 (left)) and experiment (Fig. 16 (right)) are presented. The simulation of the cohesive contact zone is well presented in Fig. 17. Fig. 17 shows the deflection of laminate 1E; it also shows a suitable damage model combined with the failure principle used to model the

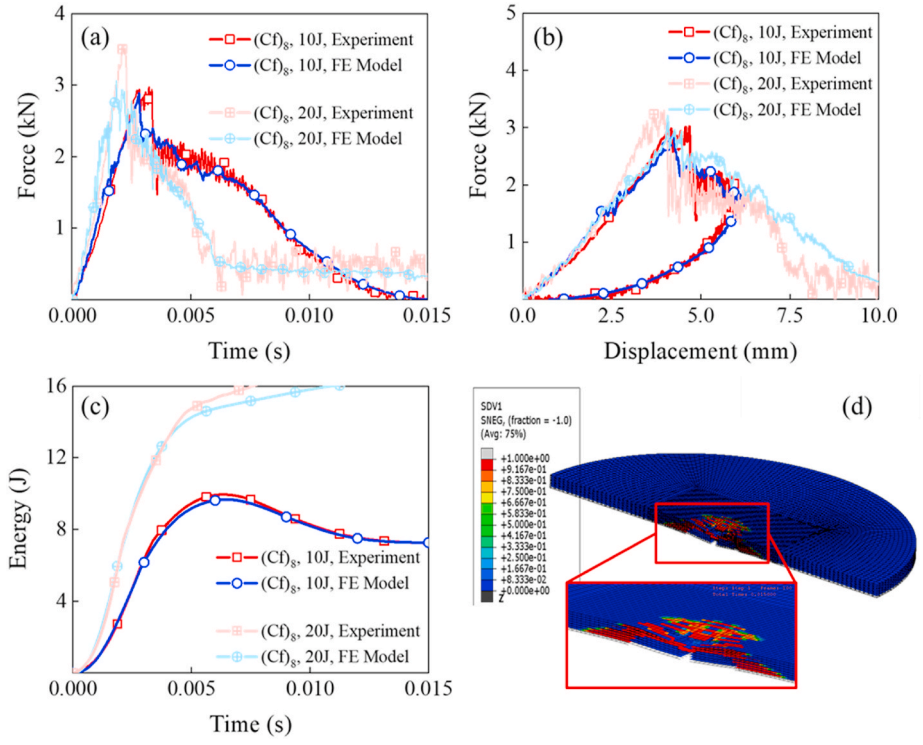

Fig. 15. Force versus time (a), force versus displacement (b), energy versus time (c), and tensile damage/failure of warp fibers (d) for the carbon FRPC laminate (1E) at 10 J and 20 J.

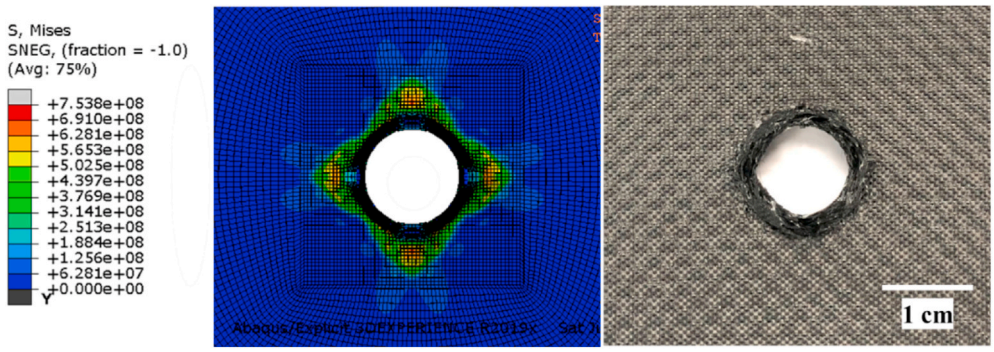

Fig. 16. The rear side of the thermoplastic carbon-based FRPC laminate (1E) at 20 J at the end of the impact FE model and experiment (plastic strain repartition).

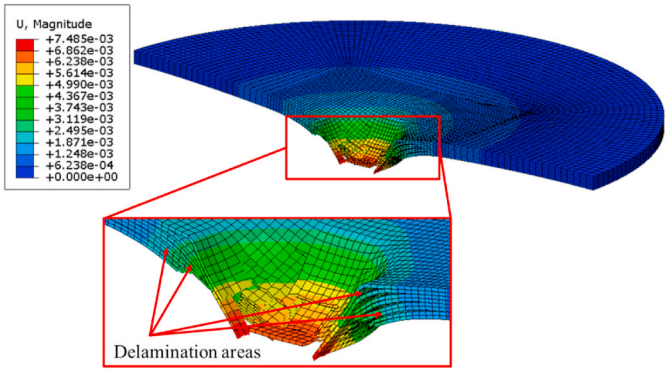

Fig. 17. Displacement (m) and delamination areas of the thermoplastic carbon FRPC laminate (1E) at 20 J.

interlaminar damaged area (delamination) in the laminate.

4. conclusion

In this study, the roles of fiber type and stacking sequence on the dynamic response of newly developed thermoplastic (TP) fiber-reinforced polymer composite (FRPC) laminates under low-velocity impact (LVI) testing were investigated. For this end, FRPCs comprising woven ultra-high molecular weight polyethylene (UHMWPE) fabrics, woven carbon fabrics, and two different hybrid systems are fabricated at ambient temperature with a novel liquid thermoplastic resin, Elium® 188. In addition, two thermosetting (TS) epoxy resins are applied for fabricating equivalent composite laminates to investigate the role of resin type on the LVI behavior of the composite structures. Different impact energy levels are performed on various TP and TS FRPC laminates to study the contact force, displacement, energy attributes, structural integrity index, and failure/damage modes. The results demonstrate that the hybrid system with UHMWPE fabrics on top and bottom can decrease the structural loss and absorbed energy up to 47% and 18%, respectively compared to the hybrid system with carbon fabrics on the sides, as UHMWPE fibers enjoy higher strain to failure. Furthermore, the ratio of energy to force absorption for the hybrid laminate with carbon fabrics on the sides can decrease from 3.7 to 2.9 by changing the stacking sequence and replacing those (side) carbon fabrics with UHMWPE fabrics. By comparing the effect of resin type on the LVI response of traditional TS laminates and the newly developed TP laminate, it was found that the TP laminate underwent extended plasticity and showed a ductile behavior, which resulted in a lower structural loss (up to 200%), a lower contact force by 14%, and lower absorbed energy by 48% compared to those presented by the TS counterparts. Moreover, the ratio of energy to force absorption for the TS laminates can decrease from 3.8 up to 2.0 by replacing the TS matrix with a thermoplastic one. Besides, the Mechanics of Structure Genome (MSG) and the commercial finite element code ABAQUS are used and the experimental results were verified. It was found that thermosetting and traditional (solid) thermoplastic resins can be replaced with the liquid thermoplastic resin, Elium®, to fabricate (hybrid) composite structures for impact applications with the advantage of manufacturing at room temperature, eliminating the residual thermal stresses, increasing the production rate, recyclability, and saving the labor and production costs.

CRediT authorship contribution statement

M.E. Kazemi: Conceptualization, Methodology, Writing – original draft. **Logesh Shanmugam:** Methodology, Writing - review & editing. **Ali Dadashi**: Theoretical Investigation. **Meisam Shakouri**: Theoretical Investigation. **Dong Lu**: Results Validation and Funding acquisition. **Zhuang Du**, **You Hu**, and **Jiasheng Wang**: Results Validation and Funding acquisition. **Weizhao Zhang:** Experimental Investigation, Funding acquisition **Lei Yang**: Validation, Supervision. **Jinglei Yang**: Conceptualization, Funding acquisition, Supervision, Writing - review & editing.

Declaration of competing interest

The authors declare that they have no known competing financial interests or personal relationships that could have appeared to influence the work reported in this paper.

Acknowledgments

The authors are grateful for the support from The Hong Kong University of Science and Technology (Grant #: R9365), the NSFC-RGC/HK Joint Research Scheme, (Grant#: N_HKUST 631/18), and Nanhai-HKUST Program (Grant #: FSNH-18FYTRI01), Guangzhou Municipal Science and Technology Bureau (Project #: 201907010024), and Science and Technological Bureau of Guangzhou Huangpu District (Project #: 2018GH04). The authors also would like to acknowledge Dr. Brian Dong and Dr. Jinchun Zhu of Arkema, Changshu Research and Development Center, China for providing Elium® resin.

References

[1] Bhudolia SK, Joshi SC, Bert A, Gohel GR, Raama M. Energy characteristics and failure mechanisms for textile spread tow thin ply thermoplastic composites under low-velocity impact. Fibers Polym 2019;20(8):1716–25.
[2] Wu Z, Zhang L, Ying Z, Ke J, Hu X. Low-velocity impact performance of hybrid 3D carbon/glass woven orthogonal composite: experiment and simulation. Compos B Eng 2020;196:108098.
[3] Damghani M, Ersoy N, Piorkowski M, Murphy A. Experimental evaluation of residual tensile strength of hybrid composite aerospace materials after low velocity impact. Compos B Eng 2019;179:107537.
[4] Quan D, Bologna F, Scarselli G, Ivanković A, Murphy N. Mode-II fracture behaviour of aerospace-grade carbon fibre/epoxy composites interleaved with thermoplastic veils. Compos Sci Technol 2020;191:108065.

[5] Zhang W, Gao J, Cao J. Blank geometry design for carbon fiber reinforced plastic (CFRP) preforming using finite element analysis (FEA). Procedia Manuf 2020;48:197–203.
[6] Kazemi ME, Kouchakzadeh MA, Shakouri M. Stability analysis of generally laminated conical shells with variable thickness under axial compression. Mech Adv Mater Struct 2018:1–14.
[7] Sierakowski RL, Telitchev IY, Zhupanska OI. On the impact response of electrified carbon fiber polymer matrix composites: effects of electric current intensity and duration. Compos Sci Technol 2008;68(3):639–49.
[8] Bunea M, Cîrciumaru A, Buciumeanu M, Bîrsan IG, Silva FS. Low velocity impact response of fabric reinforced hybrid composites with stratified filled epoxy matrix. Compos Sci Technol 2019;169:242–8.
[9] Cihan M, Sobey AJ, Blake JIR. Mechanical and dynamic performance of woven flax/E-glass hybrid composites. Compos Sci Technol 2019;172:36–42.
[10] Hosur MV, Adbullah M, Jeelani S. Studies on the low-velocity impact response of woven hybrid composites. Compos Struct 2005;67(3):253–62.
[11] Shanmugam L, Kazemi ME, Li Z, Luo W, Xiang Y, Yang L, et al. Low-velocity impact behavior of UHMWPE fabric/thermoplastic laminates with combined surface treatments of polydopamine and functionalized carbon nanotubes. Composites Commun 2020;22:100527.
[12] Kazemi ME, Shanmugam L, Li Z, Ma R, Yang L, Yang J. Low-velocity impact behaviors of a fully thermoplastic composite laminate fabricated with an innovative acrylic resin. Compos Struct 2020:112604.
[13] Kazemi ME, Shanmugam L, Lu D, Wang X, Wang B, Yang J. Mechanical properties and failure modes of hybrid fiber reinforced polymer composites with a novel liquid thermoplastic resin. Elium®. Compos Part A: Appl Sci Manuf 2019;125:105523.
[14] Kazemi ME, Shanmugam L, Chen S, Yang L, Yang J. Novel thermoplastic fiber metal laminates manufactured with an innovative acrylic resin at room temperature. Compos Appl Sci Manuf 2020;138:106043.
[15] Liu X, Rouf K, Peng B, Yu W. Two-step homogenization of textile composites using mechanics of structure genome. Compos Struct 2017;171:252–62.
[16] Bhudolia SK, Joshi SC. Low-velocity impact response of carbon fibre composites with novel liquid Methylmethacrylate thermoplastic matrix. Compos Struct 2018;203:696–708.
[17] Ali M, Joshi SC. Damage evolution in glass/epoxy composites engineered using core–shell microparticles under impact loading. J Mater Sci 2013;48(24):8354–67.
[18] Ghasemi Nejhad MN, Parvizi-Majidi A. Impact behaviour and damage tolerance of woven carbon fibre-reinforced thermoplastic composites. Composites 1990;21(2):155–68.
[19] Vieille B, Casado VM, Bouvet C. About the impact behavior of woven-ply carbon fiber-reinforced thermoplastic- and thermosetting-composites: a comparative study. Compos Struct 2013;101:9–21.
[20] Liu D. Characterization of impact properties and damage process of glass/epoxy composite laminates. J Compos Mater 2004;38(16):1425–42.
[21] Abrate S. Impact engineering of composite structures. Springer Science & Business Media; 2011.
[22] Matadi Boumbimba R, Coulibaly M, Khabouchi A, Kinvi-Dossou G, Bonfoh N, Gerard P. Glass fibres reinforced acrylic thermoplastic resin-based tri-block copolymers composites: low velocity impact response at various temperatures. Compos Struct 2017;160:939–51.
[23] Forquin P, Nasraoui M, Rusinek A, Siad L. Experimental study of the confined behaviour of PMMA under quasi-static and dynamic loadings. Int J Impact Eng 2012;40–41:46–57.
[24] Yu W, Liu X. Swiftcomp 2017.
[25] Schwab M, Todt M, Wolfahrt M, Pettermann HE. Failure mechanism based modelling of impact on fabric reinforced composite laminates based on shell elements. Compos Sci Technol 2016;128:131–7.
[26] Kinvi-Dossou G, Matadi Boumbimba R, Bonfoh N, Koutsawa Y, Eccli D, Gerard P. A numerical homogenization of E-glass/acrylic woven composite laminates: application to low velocity impact. Compos Struct 2018;200:540–54.
[27] Johnson AF. Modelling fabric reinforced composites under impact loads. Compos Appl Sci Manuf 2001;32(9):1197–206.
[28] Pinho ST, Robinson P, Iannucci L. Fracture toughness of the tensile and compressive fibre failure modes in laminated composites. Compos Sci Technol 2006;66(13):2069–79.
[29] Caputo F, De Luca A, Lamanna G, Borrelli R, Mercurio U. Numerical study for the structural analysis of composite laminates subjected to low velocity impact. Compos B Eng 2014;67:296–302.
[30] Shi Y, Soutis C. A finite element analysis of impact damage in composite laminates. Aeronaut J 2012;116(1186):1331–47.
[31] Aymerich F, Dore F, Priolo P. Prediction of impact-induced delamination in cross-ply composite laminates using cohesive interface elements. Compos Sci Technol 2008;68(12):2383–90.
[32] Zhang J, Zhang X. Simulating low-velocity impact induced delamination in composites by a quasi-static load model with surface-based cohesive contact. Compos Struct 2015;125:51–7.
[33] Shi Y, Swait T, Soutis C. Modelling damage evolution in composite laminates subjected to low velocity impact. Compos Struct 2012;94(9):2902–13.